Supplement of

Heavy precipitation-induced Yangtze River runoff greatly regulates heterotrophic prokaryotes production and induces P-limited growth in the northern East China Sea

Yong-Jae Baek[1,2,3], Bomina Kim[1,4], Seok-Hyun Youn[5], Sang-Heon Lee[6], Hyo-Keun Jang[5,6], Heejun Han[3], Hugh W. Ducklow[7], Sung-Han Kim[2,3] and Jung-Ho Hyun[1*]

[1]Department of Marine Science & Convergence Technology, Hanyang University (ERICA), 55 Hanyangdaehak-ro, Sangnok-gu, Ansan, Gyeonggi-do 15588, Republic of Korea
[2]Department of Convergence Study on the Ocean Science and Technology, Ocean Science and Technology School, Busan 49111, Republic of Korea
[3]Marine Environmental Research Department, Korea Institute of Ocean Science and Technology, Busan 49111, Republic of Korea
[4]Southeast Sea Fisheries Research Institute, National Institute of Fisheries Science, Tongyeong 53085, Republic of Korea
[5]Oceanic Climate & Ecology Research Division, National Institute of Fisheries Science, Busan 46083, Republic of Korea
[6]Department of Oceanography and Marine Research Institute, Pusan National University, Busan 46241, Republic of Korea
[7]Department of Earth and Environmental Sciences and Lamont-Doherty Earth Observatory, Columbia University, Palisades, NY 10964, USA.

Correspondence to: Jung-Ho Hyun (hyunjh@hanyang.ac.kr)

Materials and methods

Text S1. FDOM analysis method

For measuring the fluorescence spectra of fluorescent dissolved organic matter (FDOM) samples, a Hitachi F-7100 fluorescence spectrophotometer (Hitachi, Tokyo, Japan) was used. Excitation-emission matrix spectroscopy (EEMS) analysis was performed by measuring excitation wavelengths (Ex) from 250 to 500 nm (5 nm intervals) and emission wavelengths (Em) from 300 to 500 nm (5 nm intervals) with an integration time of 0.1 s. To prevent the inner filter effect, absorbance at 254 nm was checked; it stayed below 0.3 for all samples, thus no dilution was needed (Burdige et al., 2004). Scanning was conducted using a Lambda 365 UV/vis spectrophotometer (Perkin Elmer, Norwalk, USA). Milli-Q water EEMS data were used for blank subtraction and for normalizing fluorescence intensity into Raman units (R.U.) (Lawaetz and Stedmon, 2009). Parallel factor analysis (PARAFAC) was performed on 460 sets of EEMS data using MATLAB R2024a software (MathWorks Inc, Natick, USA) with the DOMFluor toolbox (Stedmon and Bro, 2008). Rayleigh and Raman scatter bands (±20 nm) were removed and replaced with missing values ("NaN" in MATLAB). Validation of the 3-component PARAFAC model was conducted through split-half validation and random initialization (Stedmon and Bro, 2008), both showing a percentage of explained variance of 98.1% and 98.0%, respectively. The results characterized one terrestrial humic-like (Component 1; C1) and two protein-like fluorescent components (Component 2 and 3; C2 and C3) in northern East China Sea (Fig. S5). The characterized three fluorescent components (C1

to C3) were compared with those from previous studies in the OpenFluor database, with Tucker's congruence coefficients exceeding 0.95, matching with the major components from 101, 76, and 32 studies, respectively (Table S1, https://openfluor.lablicate.com, last access: 24 September 2024) (Murphy et al., 2014). Component 1 ($FDOM_H$; Ex/Em = 250/430) is categorized as a mixture of terrestrial humic-like FDOM (peak A; Coble, 1996) and marine humic-like FDOM (peak M; Coble, 1996), and it can commonly be monitored in low salinity areas, such as the Yangtze River estuary in the East China Sea (Jiang et al., 2016; Zheng et al., 2018; Li et al., 2020; Sun et al., 2022; Ji et al., 2024). Component 2 ($FDOM_T$; Ex/Em = 280/340) is categorized as Tryptophan-like FDOM (peak T; Coble, 1996), and Component 3 ($FDOM_B$; Ex/Em = 270/300) is categorized as Tyrosine-like FDOM (peak B; Coble, 1996). The humification index (HIX) was calculated as the ratio of the fluorescence intensity area at emission wavelengths 435–480 nm to 300–345 nm, at excitation wavelength 255 nm (Zsolnay et al., 1999)

Text S2. Primary production

Phytoplankton primary production (PP) was assessed using stable carbon isotope (^{13}C) analysis, following the methodology outlined by Hama et al., (1983). Water samples were obtained from six distinct photic depths, representing 100%, 50%, 30%, 12%, 5%, and 1% penetration of surface photosynthetically active radiation (PAR), determined through the conversion of Secchi disc depth measurements at each sampling station. During the incubation experiments, water samples from each light depth were promptly transferred to 1 L polycarbonate incubation bottles equipped with optical filters (neutral density screens,

Lee Filters; Garneau et al., 2007) to replicate in-situ light conditions corresponding to the depths of sample collection. To mitigate potential grazing impacts from large zooplankton during the incubation period, 333 μm sieves were employed. Subsequently, ^{13}C-labelled sodium bicarbonate ($NaH^{13}CO_3$), comprising approximately 10% of concentrations in the ambient dissolved inorganic carbon, was introduced into the bottles containing the water samples. These inoculated samples were then incubated in a large on-deck incubator, maintaining light and temperature conditions consistent with those present at the sea surface. Incubations were terminated within 4-6 hours, followed by filtration through 25 mm GF/F filters (Whatman, 0.7 μm pore size) that had been pre-treated by combustion at 450 °C for 4 hours. After overnight exposure to HCl fumes to remove carbonate, the samples were analyzed at the Alaska Stable Isotope Laboratory, University of Alaska, Fairbanks, USA. Particulate organic carbon and the abundance of ^{13}C were measured using the Finnigan Delta + XL mass spectrometer. These data were then utilized to calculate primary production at each light depth according to the equation suggested by Hama et al., (1983). Depth-integrated primary production (mg C m^{-2} h^{-1}) was computed by applying trapezoidal integration to integrate volumetric primary production (mg C m^{-3} h^{-1}) throughout the entire photic zone. The daily PP (mg C m^{-2} d^{-1}) was determined by combining the hourly primary production observed in this study with previously reported 10-hour photoperiods per day in adjacent regional seas (Jang et al., 2018, 2021; Lee et al., 2017).

Text S3. Heterotrophic prokaryotes production

The Heterotrophic prokaryotes production (HPP) was determined by measuring the rate of protein synthesis using ^{3}H-leucine (^{3}H-leu) incorporation (Smith and Azam, 1992). Seawater samples (1.5 mL) were incubated at in situ temperature with ^{3}H-leu (final concentration, 10 nM, Perkin Elmer, NET1166005) for one hour in the dark. After incubation, cold 50% trichloroacetic acid (TCA) was added to stop the incubation, and samples were kept in the dark at room temperature for 30 minutes. Blank samples were treated similarly but with the addition of cold 50% TCA before the injection of ^{3}H-leu. After incubation, samples were centrifuged at 14,000 rpm for 10 minutes, and the supernatant was carefully extracted without disturbing the substances adhering to the tube walls. Cold 5% TCA was added to the tubes to extract the synthesized protein, and after another centrifugation at 14,000 rpm for 10 minutes, the supernatant was discarded. The remaining pellet was washed with cold 80% ethanol, followed by another centrifugation at 14,000 rpm for 10 minutes. Liquid scintillation cocktail (1.5 mL; Ultima Gold, Ultima Gold LSC Cocktail) was added to the samples, and ^{3}H radioactivity within the extracted protein was measured using a liquid scintillation counter (LKB, Rack Beta II). The working stock's radioactivity should be 4,995,000 dpm (disintegration per minute). We checked that all working stock radioactivity was within 2% of this value before use. The calculated protein synthesis rate of ^{3}H-leu (pmol leu L^{-1} h^{-1}) was converted to HPP (µg C L^{-1} d^{-1}) using a conversion factor (CF = 1.5 kg C mol leucine^{-1}; Kirchman, 1993).

Text S4. Statistics

Normality tests were performed using the Shapiro-Wilk and Kolmogorov-Smirnov tests. An independent samples t-test was carried out to compare integrated HPP within the mixed layer depth (MLD) in the spring and summer across the ECS, YS, and ES. One-way analysis of variance (ANOVA) was used to compare the means of August DOC and HPP across years, followed by Dunn's post hoc test. In cases where normality assumptions were not met, the Kruskal-Wallis H test was employed. Simple regression analysis was conducted between DOC and salinity within the MLD after confirming the normality and homoscedasticity of residuals. Correlation analyses involving HPP and DOC, $FDOM_H$ and DOC, $FDOM_H$ and salinity, and Chl-*a* and HPP were conducted using Pearson's or Spearman's rank correlation, depending on the normality of the data. A *p*-value of less than 0.05 was considered significant.

Table S1. Characteristics of three PARAFAC components

Component	Ex/Em (nm)	Coble (1996) Peaks	Similar component	Description
C1	250/430	A + M (mixture of terrestrial and marine humic-like)	C1 (Jiang et al., 2016) C4 in summer (Zheng et al., 2018) C2 (Li et al., 2020) C3 (Sun et al., 2022) C3 (Ji et al., 2024)	UVC humic-like components, characterized by high molecular weight, are related to the activity of organisms and are typically found in forest environments and wetlands
C2	280/340	T (Tryptophan-like)	C2 (Jørgensen et al., 2011) C5 (Yamashita et al., 2011) C4 (Cawley et al., 2012) C5 (Asmala et al., 2018)	UVB protein-like components, characterized by high molecular mass DOM, are predominantly derived from autochthonous processes and usually observed in surface waters
C3	270/300	B (Tyrosine-like)	C1 (Murphy et al., 2006) C6 (Yamashita et al., 2011)	Relatively lower molecular mass than tryptophan-like DOM, strongly correlates with total hydrolysable amino acids

	C4 (Kowalczuk et al., 2013)	(THAA)
	C1 (Paerl et al., 2020)	

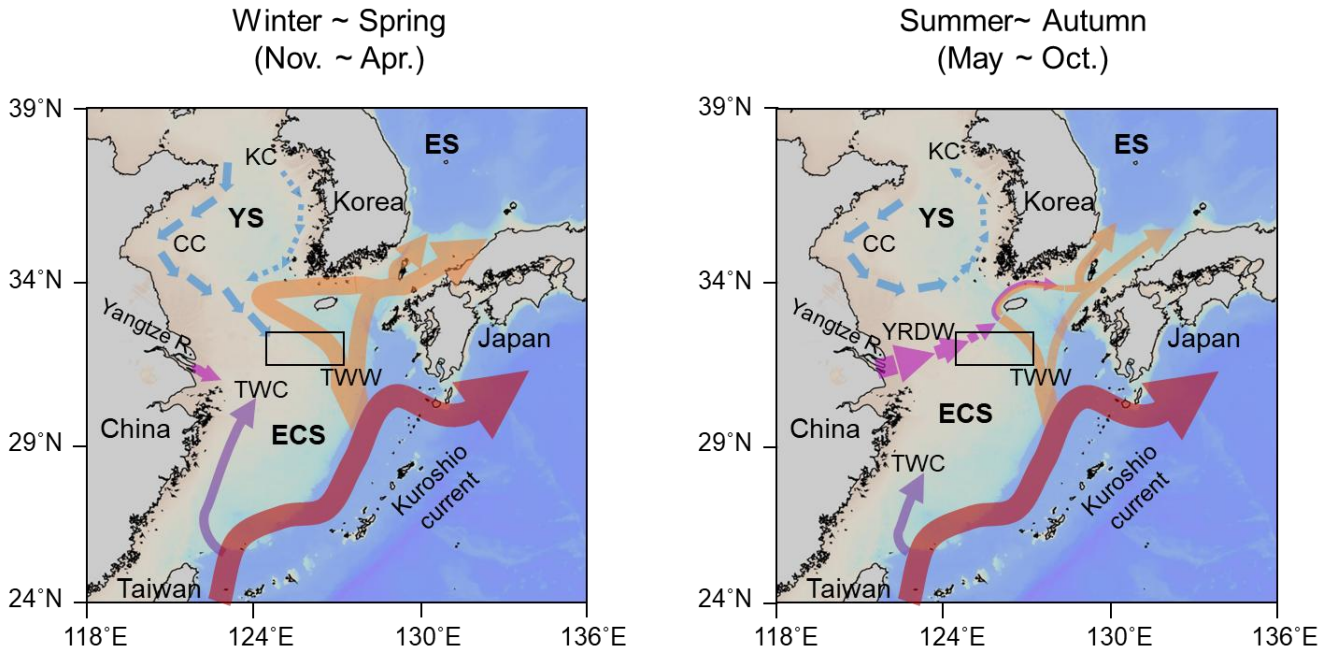

Figure S1. Seasonal surface currents of the Northwest Pacific Ocean. YS: Yellow Sea, ECS: East China Sea, ES: East Sea, CC: Chinese coastal current, KC: Korean coastal current, YRDW: Yangtze River diluted water, TWC: Taiwan warm current, TWW: Tsushima warm water. The winter season spans from November to April, and the summer season from May to October. The black box indicates the study area in the northern East China Sea. Figures were modified from Lie and Cho, (2016). Thickness of the arrows denotes magnitude of the current. The Kuroshio current delivers warm and saline water along the shelf break throughout the year. Two major branches of this current, the TWC and the TWW, transport South China Sea water into the central and nECS and subsequently toward the East Sea (Su and Weng, 1994). In winter, the CC, driven by the winter monsoon (i.e., northeasterly winds), brings cold and fresh water southward along the Chinese coast (Chu et al., 2005; Lie and Cho, 2016). In contrast, during summer, the summer monsoon (i.e., southeasterly winds) and river discharge drive the offshore expansion and long-distance transport of the YRDW toward the East Sea (Chang and Isobe, 2003).

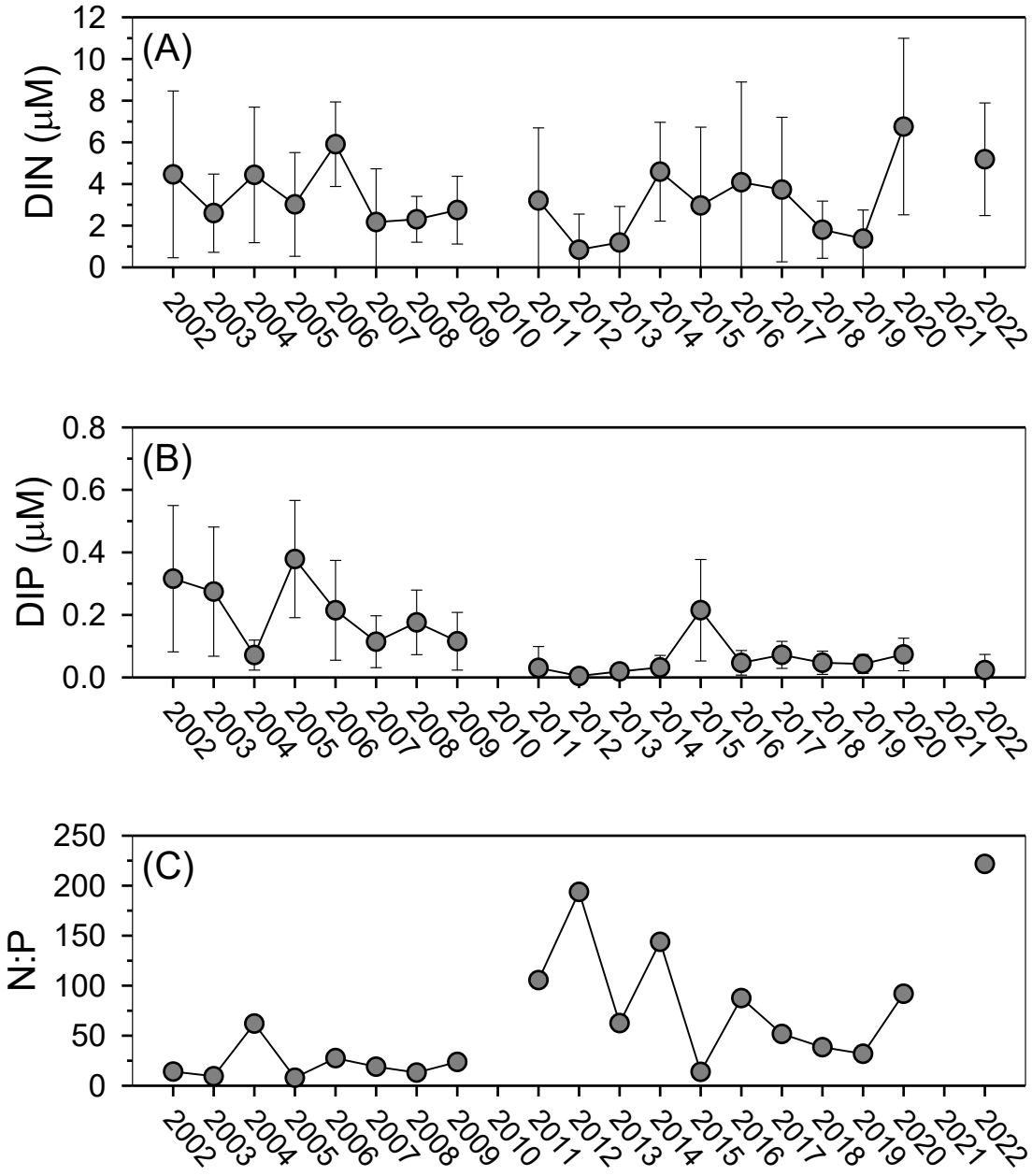

Figure S2. Long-term summer (August) nutrient data in the northern East China Sea. (A) Dissolved inorganic nitrogen (DIN), (B) dissolved inorganic phosphate (DIP), and (C) DIN to DIP ratio (N:P). Nutrient data were obtained from the Korean National Institute of Fisheries Science (NIFS) (https://www.nifs.go.kr/kodc/soo_list.kodc, last access: 05 November 2024).

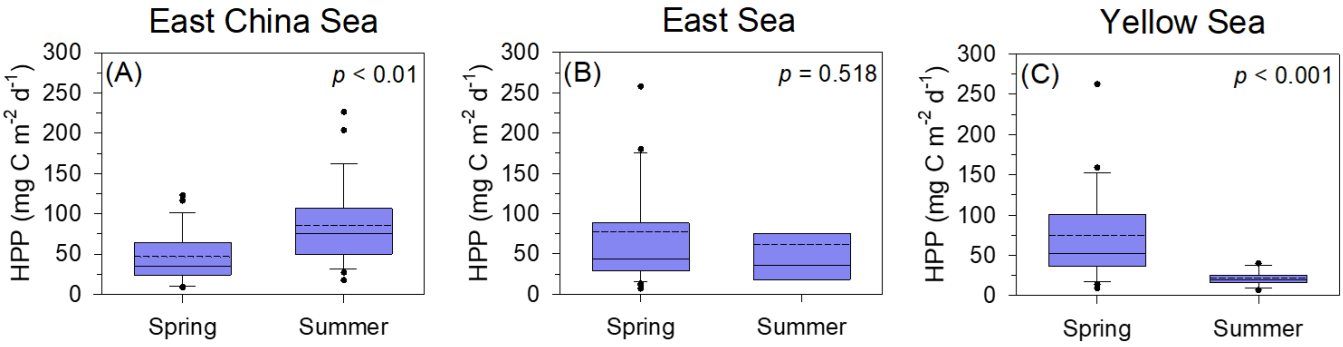

Figure S3. Comparison of integrated heterotrophic prokaryotes production (HPP) within the mixed layer depth in the East China Sea (A), the East Sea (B) and the Yellow Sea (C) during spring and summer from 1996 to 2022 (Hyun and Kim, 2003, Hyun et al., 2009; Kim et al., 2017, 2020, 2025; Hyun J-H unpublished data). The solid line indicates the median value, and the dotted line indicates the average value (sample size, n = 8 – 32).

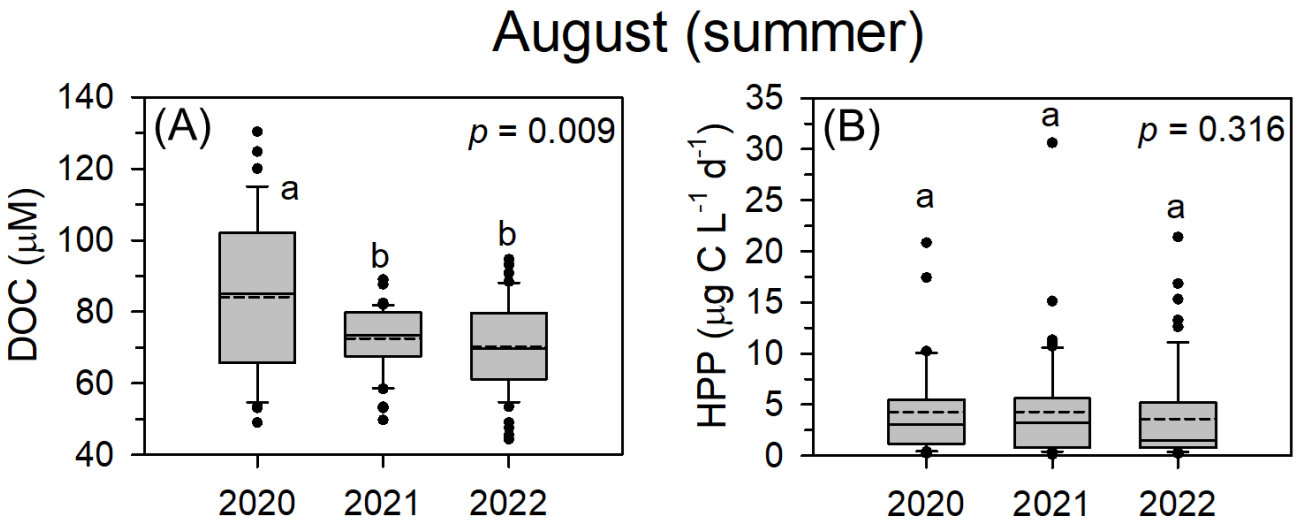

Figure S4. Box plot of dissolved organic carbon (DOC) (A) and heterotrophic prokaryotes production (HPP) (B) in August 2020 – 2022. The solid line in each box indicates the median value, and the dotted line indicates the average value (sample size, n = 36 – 55).

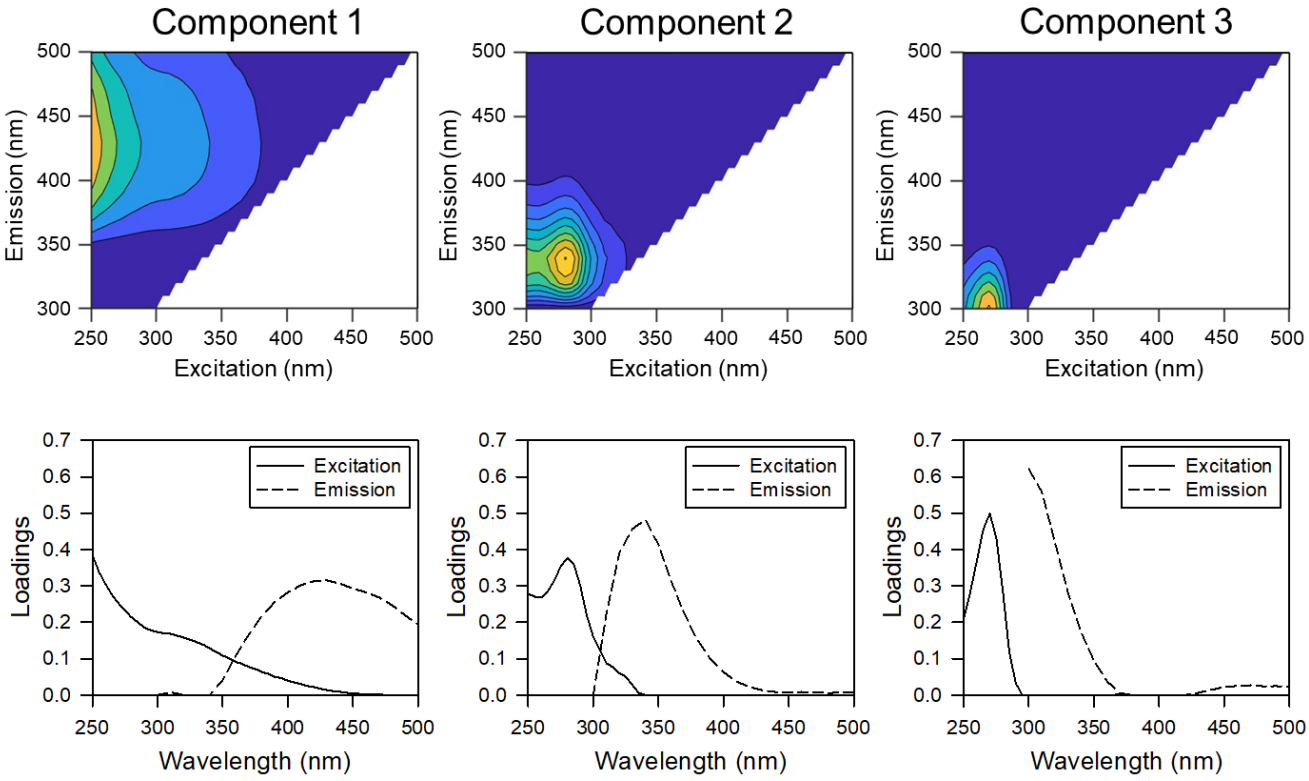

Figure S5. Contour plots of fluorescence EEM spectra and excitation-emission loadings of Component 1 (FDOM$_H$; terrestrial humic-like fluorophore), Component 2 (FDOM$_T$; Tryptophan-like fluorophore), and Component 3 (FDOM$_B$; Tyrosine-like fluorophore) determined using the PARAFAC model in the northern East China Sea.

References

Asmala, E., Haraguchi, L., Markager, S., Massicotte, P., Riemann, B., Staehr, P. A., and Carstensen, J.: Eutrophication leads to accumulation of recalcitrant autochthonous organic matter in coastal environment, Global Biogeochem. Cy., 32, 1673–1687, https://doi.org/10.1029/2017GB005848, 2018.

Burdige, D. J., Kline, S. W., and Chen, W.: Fluorescent dissolved organic matter in marine sediment pore waters, Mar. Chem., 89, 289–311, https://doi.org/10.1016/j.marchem.2004.02.015, 2004.

Cawley, K. M., Ding, Y., Fourqurean, J., and Jaffé, R.: Characterising the sources and fate of dissolved organic matter in Shark Bay, Australia: A preliminary study using optical properties and stable carbon isotopes, Mar. Freshwater Res., 63, 1098–1107, https://doi.org/10.1071/MF12028, 2012.

Chang, P.-H. and Isobe, A.: A numerical study on the Changjiang diluted water in the Yellow and East China Seas, J. Geophys. Res., 108, 3299, https://doi.org/10.1029/2002JC001749, 2003.

Chu, P., Chen, Y., and Kuninaka, A.: Seasonal variability of the Yellow Sea/East China Sea surface fluxes and thermohaline structure, Adv. Atmos. Sci., 22, 1–20, https://doi.org/10.1007/BF02930865, 2005.

Coble, P. G.: Characterization of marine and terrestrial DOM in seawater using excitation-emission matrix spectroscopy, Mar. Chem., 51, 325–346, https://doi.org/10.1016/0304-4203(95)00062-3, 1996.

Garneau, M., Gosselin, M., Klein, B., Tremblay, J. E., and Fouilland, E.: New and regenerated production during a late summer bloom in an Arctic polynya, Mar. Ecol. Prog. Ser., 345, 13–26, https://doi.org/10.3354/meps06965, 2007.

Hama, T., Miyazaki, T., Ogawa, Y., Iwakuma, T., Takahashi, M., Otsuki, A., and Ichimura, S.: Measurement of photosynthetic production of a marine phytoplankton population using a stable ^{13}C isotope, Mar. Biol., 73, 31–36, https://doi.org/10.1007/BF00396282, 1983.

Hyun, J.-H. and Kim, K.-H.: Bacterial abundance and production during the unique spring phytoplankton bloom in the central Yellow Sea, Mar. Ecol. Prog. Ser., 252, 77–88, https://doi.org/10.3354/meps252077,

2003.

Hyun, J.-H., Kim, D., Shin, C.-W., Noh, J.-H., Yang, E.-J., Mok, J.-S., Kim, S.-H., Kim, H.-C., and Yoo, S.: Enhanced phytoplankton and bacterioplankton production coupled to coastal upwelling and an anticyclonic eddy in the Ulleung Basin, East Sea, Aquat. Microb. Ecol., 54, 45–54, https://doi.org/10.3354/ame01280, 2009.

Jang, H. K., Kang, J. J., Lee, J. H., Kim, M., Ahn, S. H., Jeong, J.-Y., Yun, M. S., Han, I.-S., and Lee, S. H.: Recent primary production and small phytoplankton contribution in the Yellow Sea during the summer in 2016, Ocean Sci. J., 53, 509–519, https://doi.org/10.1007/s12601-018-0017-z, 2018. Jang, H. K., Kang, J. J., Lee, J. H., Kim, M., Ahn, S. H., Jeong, J.-Y., Yun, M. S., Han, I.-S., and Lee, S. H.: Recent primary production and small phytoplankton contribution in the Yellow Sea during the summer in 2016, Ocean Sci. J., 53, 509–519, https://doi.org/10.1007/s12601-018-0017-z, 2018.

Jang, H.-K., Youn, S.-H., Joo, H., Kim, Y., Kang, J.-J., Lee, D., Jo, N., Kim, K., Kim, M.-J., Kim, S., and Lee, S.-H.: First concurrent measurement of primary production in the Yellow Sea, the South Sea of Korea, and the East/Japan Sea, 2018, J. Mar. Sci. Eng., 9, 1237, https://doi.org/10.3390/jmse9111237, 2021.

Ji, X., Zhao, M.-L., Zhang, J., and Yang, G.-P.: Spatial variation in the optical and molecular properties of dissolved organic matter in the Yellow Sea and East China Sea, Prog. Oceanogr., 220, 103192, https://doi.org/10.1016/j.pocean.2023.103192, 2024.

Jiang, Y., Zhao, J., Li, P., and Huang, Q.: Linking optical properties of dissolved organic matter to multiple processes at the coastal plume zone in the East China Sea, Environ. Sci.-Proc. Impacts, 18, 1316–1324, https://doi.org/10.1039/c6em00341a, 2016.

Jørgensen, L., Stedmon, C. A., Kragh, T., Markager, S., Middelboe, M., and Søndergaard, M.: Global trends in the fluorescence characteristics and distribution of marine dissolved organic matter, Mar. Chem., 126, 139–148, https://doi.org/10.1016/j.marchem.2011.05.002, 2011.

Kim, B., Kim, S.-H., Kwak, J. H., Kang, C.-K., Lee, S. H., and Hyun, J.-H.: Heterotrophic bacterial

production, respiration, and growth efficiency associated with upwelling intensity in the Ulleung Basin, East Sea, Deep-Sea Res. Pt. II, 143, 24–35, https://doi.org/10.1016/j.dsr2.2017.07.002, 2017.

Kim, B., An, S. U., Kim, T. H., and Hyun, J.-H.: Uncoupling between heterotrophic bacteria and phytoplankton and changes in trophic balance associated with warming of seawater in Gyeonggi Bay, Yellow Sea, Estuaries Coasts, 43, 535–546, https://doi.org/10.1007/s12237-019-00606-1, 2020.

Kim, B., Baek, Y. J., Han, H., Lee, H., Youn, S.-H., and Hyun, J.-H.: P-limited prokaryotic heterotrophic production and metabolic balance between prokaryotic carbon demand and phytoplankton primary production in summer in the central Yellow Sea, Ocean Sci. J., 60, 14, https://doi.org/10.1007/s12601-025-00209-x, 2025.

Kirchman, D. L.: Leucine incorporation as a measure of biomass production by heterotrophic bacteria, in: Handbook of Methods in Aquatic Microbial Ecology, edited by: Kemp, P. F., Sherr, B. F., Sherr, E. B., and Cole, J. J., Lewis Publishers, Boca Raton, USA, 700–709, 1993.

Kowalczuk, P., Tilstone, G. H., Zabłocka, M., Röttgers, R., and Thomas, R.: Composition of dissolved organic matter along an Atlantic Meridional Transect from fluorescence spectroscopy and Parallel Factor Analysis, Mar. Chem., 157, 170–184, https://doi.org/10.1016/j.marchem.2013.10.004, 2013.

Lawaetz, A. J. and Stedmon, C. A.: Fluorescence intensity calibration using the Raman scatter peak of water, Appl. Spectrosc., 63, 936–940, https://doi.org/10.1366/000370209788964548, 2009.

Lee, S. H., Joo, H., Lee, J. H., Lee, D. W., Kang, Y. S., and Kang, C. K.: Seasonal carbon uptake rates of phytoplankton in the northern East/Japan Sea, Deep-Sea Res. Pt. II, 143, 45–53, https://doi.org/10.1016/j.dsr2.2017.04.009, 2017.

Li, M., Xie, W., Li, P., Yin, K., and Zhang, C.: Establishing a terrestrial proxy based on fluorescent dissolved organic matter from sediment pore waters in the East China Sea, Water Res., 182, 116005, https://doi.org/10.1016/j.watres.2020.116005, 2020.

Lie, H.-J. and Cho, C.-H.: Seasonal circulation patterns of the Yellow and East China Seas derived from

satellite-tracked drifter trajectories and hydrographic observations, Prog. Oceanogr., 146, 121–141, https://doi.org/10.1016/j.pocean.2016.06.004, 2016.

Murphy, K. R., Stedmon, C. A., Wenig, P., and Bro, R.: OpenFluor: An online spectral library of auto-fluorescence by organic compounds in the environment, Anal. Methods-UK, 6, 658–661, https://doi.org/10.1039/c3ay41935e, 2014.

Murphy, K. R., Ruiz, G. M., Dunsmuir, W. T. M., and Waite, T. D.: Optimized parameters for fluorescence-based verification of ballast water exchange by ships, Environ. Sci. Technol., 40, 2357–2362, https://doi.org/10.1021/es0519381, 2006.

Paerl, R. W., Claudio, I. M., Shields, M. R., Bianchi, T. S., and Osburn, C. L.: Dityrosine formation via reactive oxygen consumption yields increasingly recalcitrant humic-like fluorescent organic matter in the ocean, Limnol. Oceanogr. Lett., 5, 337–345, https://doi.org/10.1002/lol2.10154, 2020.

Smith, D. C. and Azam, F.: A simple, economical method for measuring bacterial protein synthesis rates in seawater using 3H-leucine, Mar. Microb. Food Webs, 6, 107–114, 1992.

Stedmon, C. A. and Bro, R.: Characterizing dissolved organic matter fluorescence with parallel factor analysis: A tutorial, Limnol. Oceanogr.-Meth., 6, 572–579, https://doi.org/10.4319/lom.2008.6.572, 2008.

Su, Y.-S. and Weng, X.-C.: Water masses in China Seas, in: Oceanology of China Seas, Vol. 2, edited by: Di, Z., Yuan-Bo, L., and Cheng-Kui, Z., Springer, Dordrecht, the Netherlands, 17–28, https://doi.org/10.1007/978-94-011-0862-1_2, 1994.

Sun, X., Li, P., Zhou, Y., He, C., Cao, F., Wang, Y., Shi, Q., and He, D.: Linkages between optical and molecular signatures of dissolved organic matter along the Yangtze River Estuary-to-East China Sea continuum, Front. Mar. Sci., 9, 933561, https://doi.org/10.3389/fmars.2022.933561, 2022.

Yamashita, Y., Panton, A., Mahaffey, C., and Jaffé, R.: Assessing the spatial and temporal variability of dissolved organic matter in Liverpool Bay using excitation-emission matrix fluorescence and parallel factor analysis, Ocean Dynam., 61, 569–579, https://doi.org/10.1007/s10236-010-0365-4, 2011.

Zheng, H., Yan, Z., Chen, J., Jin, H., Chen, C.-T. A., Liu, M., Yan, Z., and Ji, Z.: Seasonal variations of dissolved organic matter in the East China Sea using EEM-PARAFAC and implications for carbon and nutrient cycling, Sustainability, 10, 1444, https://doi.org/10.3390/su10051444, 2018.

Zsolnay, A., Baigar, E., Jimenez, M., Steinweg, B., and Saccomandi, F.: Differentiating with fluorescence spectroscopy the sources of dissolved organic matter in soils subjected to drying, Chemosphere, 38, 45–50, https://doi.org/10.1016/S0045-6535(98)00166-0, 1999.